INFLUENCE OF SPIRO-OMETAD FILM THICKNESS ON THE STRUCTURAL AND ELECTRICAL PROPERTIES OF PEROVSKITE SOLAR CELLS

Tazhibayev S.K.[1], Alekseev A.M.[2], Aimukhanov A.K.[1], Ilyassov B.R.[3],
Beisembekov M.K.[1], Rozhkova X.S.[1], Mussabekova A.K.[1], Zeinidenov A.K.[1]*

[1] E.A. Buketov Karagandy University, Karaganda, Kazakhstan
[2] Kazan Federal University, Kazan, Russia
[3] Astana IT University, Expo C1, Astana, Kazakhstan
Corresponding authors: a.k.zeinidenov@gmail.com

Abstract. *This work investigates the effect of the hole transport layer (HTL) thickness of Spiro-OMeTAD on the electrical transport properties in perovskite solar cells (PSCs). Spiro-OMeTAD films were obtained by the spin-coating method at centrifuge rotation speeds from 2000 to 7000 rpm. The thickness and morphology of the Spiro-OMeTAD films were studied by atomic force microscopy (AFM). From the obtained AFM image data, an increase in the surface root mean square (rms) value is observed with decreasing film thickness. A decrease in film thickness leads to an increase in Energy gap (E_g) from 2.97 eV to 3.01 eV. We observe that at a layer thickness of 260 nm, the efficiency of the cells reaches its maximum value; further increasing the layer thickness reduces the efficiency. Analysis of the impedance spectra of PSCs showed that the optimal layer thickness reduces the HTL resistance and increases the recombination resistance at the perovskite/HTL interface, which increases the effective lifetime of charge carriers. Images of the surface and current distribution of Spiro-OMeTAD on the surface of the perovskite layer were studied. A non-uniform current distribution on the surface of the samples was revealed, the observed spots with high conductivity are interpreted as perovskite quantum dots, which have better photovoltaic characteristics.*

Keywords: Perovskite solar cells, hole transport layer, Spiro-OMeTAD, conductive-AFM, current-voltage characteristics, impedance measurements.

1. Introduction

In recent years, organic-inorganic perovskite solar cells have attracted much attention from the global scientific community. The unprecedented development of PSCs is driven by their high optical absorption coefficient, tunable bandgap, low cost, ease of fabrication, and great potential to achieve higher efficiency compared to c-Si solar cells [1–3]. To increase the efficiency and stability of PSCs, work is being done to search and optimize the composition of all parts of the solar cell, not only the perovskite itself, but also the so-called transport layers. The hole-conducting transport layer plays an important role in the efficiency of charge transfer and extraction of photoexcited perovskite, HTL is important for power conversion efficiency (PCE) and stability in PSCs. Transport layers typically consist of small organic molecules, polymers, or inorganic materials such as oxides. The energy level of the HTL material must coincide with the maximum

of the perovskite valence band. The difference between these two energy levels allows for hole transport, but too large a difference in energy levels can lead to energy loss [4-6]. Thus, when using a hole transport material in PSCs, various basic requirements must be met, such as solubility, suitable energy level, and high hole mobility [7]. The organic molecule Spiro-OMeTAD (2,20,7,70-tetrakis (N, N-di-p-methoxyphenylamine)-9,90-spirobifluorene) is the most abundant HTL material in PSCs. This is due to its suitable glass transition temperature, high transparency in the visible spectrum and almost perfect energy band matching with $MAPbI_3$ [8, 9]. The Spiro-OMeTAD layer above the photoactive layer is used as an HTL to block electrons and pass holes to the bottom electrode. In addition to transporting holes into PSCs, Spiro-OMeTAD avoids direct contact between the photoactive layer and the bottom electrode. Currently, the efficiency of converting light energy into electrical energy in PSCs exceeds 25%. These indicators were obtained as before using HTL based on Spiro-OMeTAD [10,11].

Studies have shown that charge transport properties at the perovskite/HTL interface are the main factor limiting the efficiency and stability of high-performance PSCs [12,13]. It was shown in [14] that recombination between holes in HTL and electrons in perovskite is the main mechanism of recombination losses in PSCs. The amount of interfacial recombination can be influenced by the electronic coupling between the HTL and the perovskite, the number of trap states in the HTL, and the conductivity of the HTL [15–17]. Fast charge transfer through HTL is also important for the efficiency of PSCs; the conductivity of hybrid perovskites is orders of magnitude higher than that of used HTLs, which can cause the accumulation of high hole densities at the interface [18]. Therefore, the reduction in the transit time of charges through the HTL can be increased due to the optimal thickness of the HTL, or by increasing its conductivity by doping with various materials, which will significantly improve both the fill factor (FF) and V_{oc} of the device by improving charge extraction and reducing the probability of passage recombination in HTL [19]. Various thicknesses of perovskite and HTM layers have been reported, and an optimal value is required for each layer. A thick perovskite layer greater than 1000 nm results in decreased hole collection efficiency due to increased resistance and recombination within the perovskite layer. Thin perovskite layers less than 100 nm cause low photocurrent due to lower photo-absorption. The likelihood of recombination is reduced because the holes travel a shorter distance to reach the electrode. Device performance improves when using a thinner HTM. The probability of hole accumulation depends on the thickness of the HTL. Therefore, an ideal HTL thickness is required for a high-performance device. In addition, since the perovskite surface contains crystallites, which can protrude through the HTM and contact the electrode if a very thin HTL is used [20, 21]. In addition to this, concomitant light absorption by HTL can also reduce the efficiency of PSCs by negatively affecting the short-circuit current density (J_{sc}) [22]. Therefore, ideal HTL thickness is required for high-performance PSCs.

Thus, the use of Spiro-OMeTAD as HTL is extremely popular for perovskite solar cells, making the study of charge transfer and recombination dynamics at the perovskite/HTL interface a highly relevant task. Optimizing the thickness of the hole transport layer is an important procedure for the fabrication of high-performance PSCs. Despite the fact that work has already been carried out around the world to optimize the thickness of HTL, studies that include various characterization methods that provide a complete understanding of the processes of hole transport in PSCs remain relevant. In this work, we fabricated Spiro-OMeTAD-based solar cells and studied the effect of HTL thickness on the electrical transport performance in PSCs.

2. Experimental part. Materials and Methods

2.1. Sample preparation and deposition process

Solar Cell Fabrication. Perovskite solar cells were constructed on glass substrates coated with a thin conductive layer of FTO (15 Ohm/cm^2), which acted as an external electrode (cathode). A TiO_2 film (Ti-Nanoxide BL/SC-Solaronix) was applied to the surface of the FTO substrate using the spin-coating method from a solution at a rotation speed of 5000 rpm, followed by annealing at a temperature of 500°C for 60 minutes. Next, a perovskite layer and a Spiro-MeOTAD hole-transport layer were sequentially deposited on the TiO_2 surface. Spiro-OMeTAD films were obtained at different centrifuge speeds of 2000, 3000, 4000, 5000, 6000 and 7000 rpm. Finally, an Ag electrode was deposited onto the surface of the films in a vacuum atmosphere at a pressure of 10^{-3} Pa.

Perovskite Materials. $PbCl_2$ (Sigma Aldrich) and Methylammonium iodide (MAI, Sigma Aldrich) were used to prepare perovskite. Solutions were prepared by dissolving weighed portions of $PbCl_2$ (230 mg) and

MAI (394 mg) powder in 1 ml of N, N-Dimethylformamide (Sigma Aldrich). The resulting solution was stirred on a magnetic stirrer at a temperature of 60°C for 2 hours. To ensure complete crystallization, after deposition, the perovskite films were annealed for 2 hours at 100 °C. The crystallization process is accompanied by a change in the color of the film from yellow to dark brown.

Composition of HTM. The hole transport layer was made from 1 ml chlorobenzene (Sigma Aldrich) and 75 mg Spiro–OMeTAD. The resulting solution was stirred on a magnetic stirrer at a temperature of 30°C for 1 hour. To reduce the oxidation process, all operations were carried out in a sealed glove box with an inert atmosphere. Structural formulas (a) and a scheme for producing perovskite solar cells (b) are shown in Fig.1.
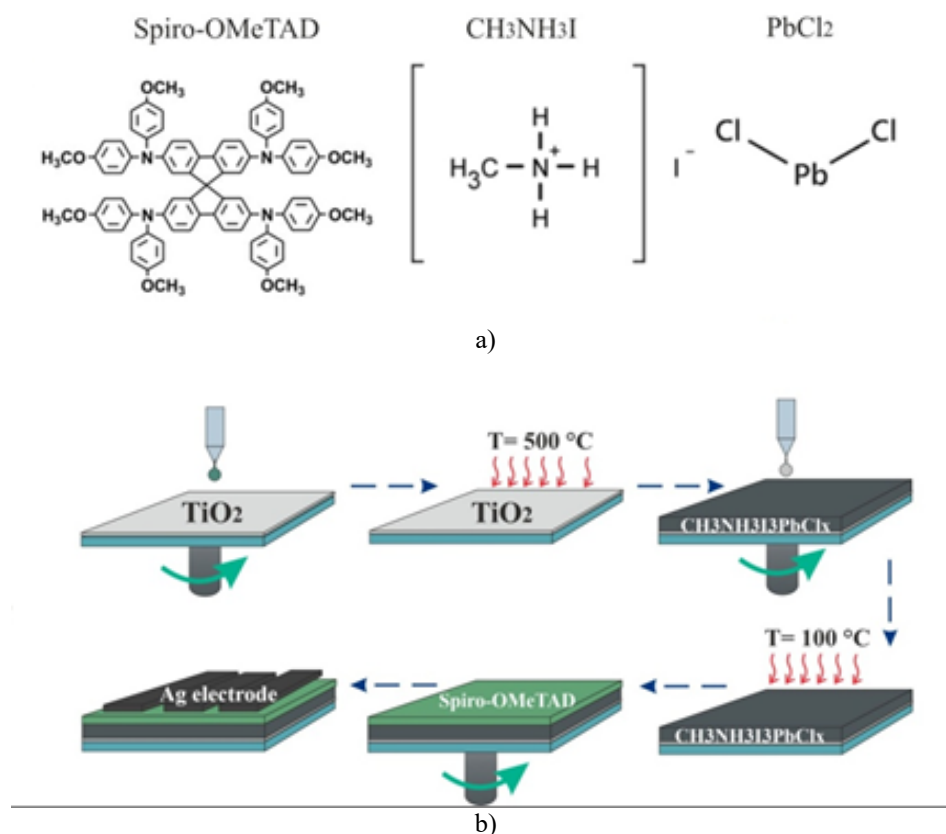

a)

b)

Fig.1. Structural formula (a) and preparation scheme perovskite solar cells (b)

2.2. Analysis methods

The surface topography and thickness of the samples were studied using a JSPM-5400 atomic force microscope (AFM, JEOL). To process the AFM images, a modular program for analyzing scanning probe microscopy data (Win SPMII Data-Processing Software) was used. A SolverP47 (NT-MDT) AFM was used to measure the local current distribution. When measuring current, a voltage was applied to the sample, while a conductive probe coated with a gold film was grounded. To measure surface topography and determine rms, a semi-contact scanning mode was used (NSC14 probe, Micromash); current measurements were carried out in contact mode (CSC37/Au probe, Micromash). The thickness of the deposited layers and the distribution of PSCs elements were measured using a scanning electron microscope (SEM, MIRA 3 LMU, Tescan). The absorption spectra of Spiro-OMeTAD thin films were investigated on an AvaSpec-ULS2048CL-EVO spectrometer (Avantes). A combined deuterium-halogen light source AvaLight-DHc (Avantes) with a working range of 200-2500 nm was used as probing radiation.

Thermal deposition of films was carried out using a vacuum deposition machine CY-1700x-spc-2 (Zhengzhou CY Scientific Instruments Co., Ltd). The preparation and assembly processes of PSCs were carried out in a glove box with an inert atmosphere. Impedance spectra were measured using a P45X potentiostat-galvanostat in impedance mode. The current-voltage characteristics of photosensitive cells were determined using a Sol3A Class AAA Solar Simulators (Newport) with PVIV-1A I-V Test Station device.

3. Results and Discussion

3.1. Structural analysis of the prepared films

Figure 2 shows AFM images of the surface of the HTL layer of Spiro-OMeTAD, obtained at different centrifuge rotation speeds. As can be seen from Figure 2a, the surface morphology of the HTL layer obtained at the lowest rotation speed is uniform and smooth. The rare pores observed are apparently associated with the evaporation of the solvent when the film dries. As the rotation speed increases, a structure with characteristic sizes of regions of several hundred nanometers appears on the surface of the film (Figures 2b-2f). The appearance of such a structure can be explained by the influence of the FTO substrate surface.
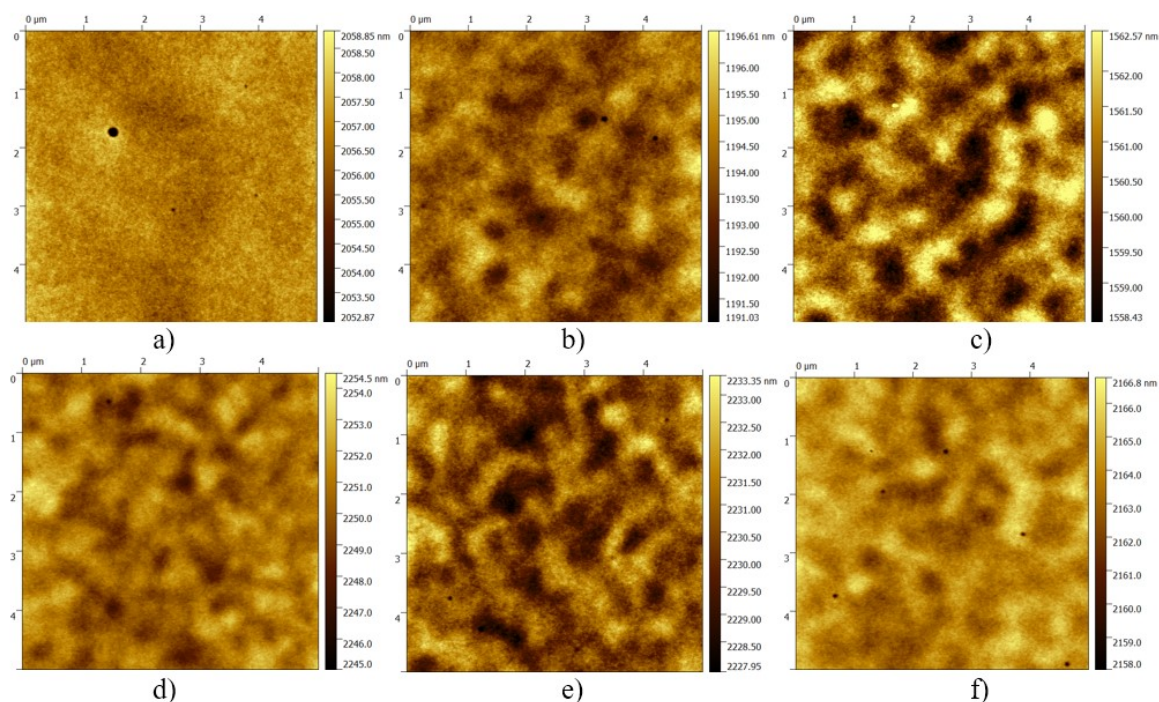

Fig.2. Surface morphology of Spiro-OMeTAD films, obtained at different substrate rotation speeds:
a) 2000 rpm.; b) 3000 rpm.; c) 4000 rpm.; d) 5000 rpm.; e) 6000 rpm.; f) 7000 rpm.

Figure 3a shows the dependence of the thickness of Spiro-OMeTAD films on the centrifuge rotation speed. The thickness was determined from the step height obtained by scratching the surface of the film by measuring the height difference using statistical analysis. The solid line in the figure shows the well-known dependence of thickness on centrifugation speed $t \sim 1/\sqrt{w}$, fitted to the data obtained using the least squares method.
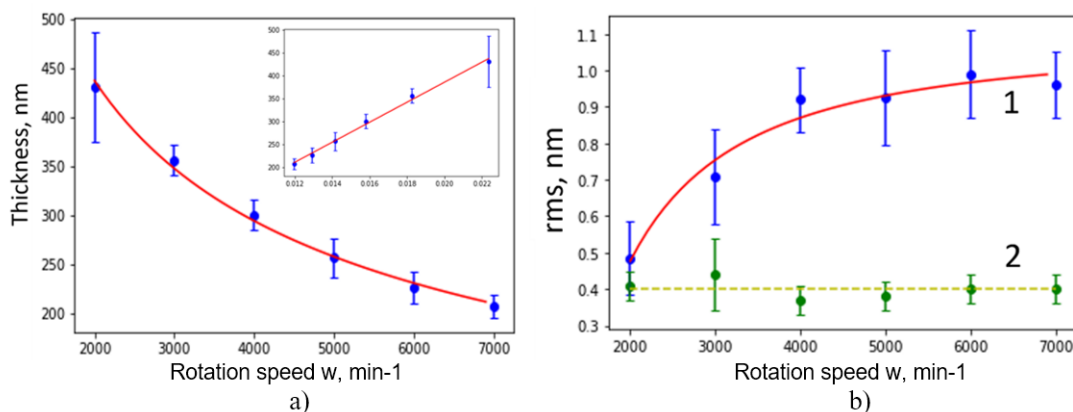

Fig.3. Thickness (a) and standard deviation (b) of the surface of the spin-coated Spiro-OMeTAD film as a function of rotation speed: a) blue symbols – experimental data, red line – dependence $t \sim 1/w^{0.5}$; in the inset - the same data in coordinates t $(1/w^{0.5})$; b) data 1 – for FTO film, data 2 – for film on glass; the lines show the average value for 2 and the $rms \sim w^{0.5}$ dependence for 1.

It can be seen that the obtained thicknesses are in good agreement with the theoretical dependence and decrease monotonically with increasing rotation speed. Apparently, as the rotation speed increases, the film thickness decreases and the structure of the substrate appears in the AFM image.

Figure 3b shows surface root mean square deviation (rms) versus spin speed for Spiro-OMeTAD films deposited on FTO and glass. For a film on FTO, a sharp increase in surface rms is observed when the rotation speed increases to 4000 rpm, then the dependence saturates. The stabilization of rms can be explained by the stabilization of thickness at high speeds: the structure of the substrate appears approximately the same for samples obtained at speeds from 4000 rpm. The rms dependence for FTO films is well approximated by the rms~$w^{0.5}$ dependence. Thus, dependences of thickness and rms on rotation speed are inverse for FTO substrate. For Spiro-OMeTAD films deposited on glass, no dependence of rms on rotation speed is observed; the average rms value of films on glass is close to the rms value of the thickest film on FTO. The SEM image of the cross-cleavage and the element distribution of PSCs are shown in Figure 4. From the figure 4, it can be seen that the thickness of the FTO film is 360 nm, the thickness of the TiO$_2$ film is 65 nm, the perovskite layer is 340 nm, the Spiro-OMeTAD layer is 260 nm, the Ag electrode layer is 70 nm.
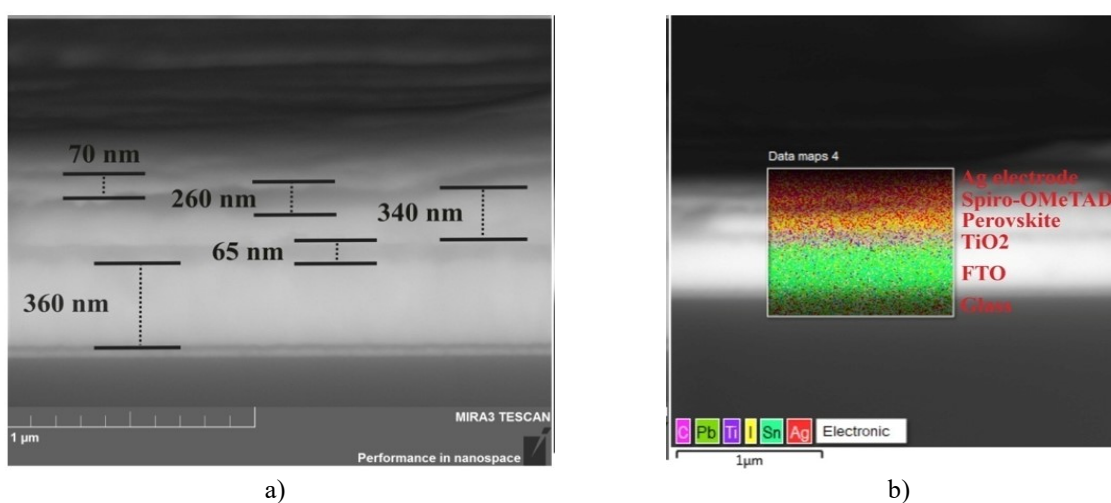

a)   b)

Fig.4. SEM images of transverse cleavage a) and distribution of PSCs elements b)

3.2. Optical properties

Figure 5a shows the absorption spectra of Spiro-OMeTAD films. The absorption spectrum of Spiro-OMeTAD has three maxima, the most intense is at a wavelength of λ=228 nm, and the other two maxima are less intense and are located at λ=308 nm and λ=373 nm.

a)   b)
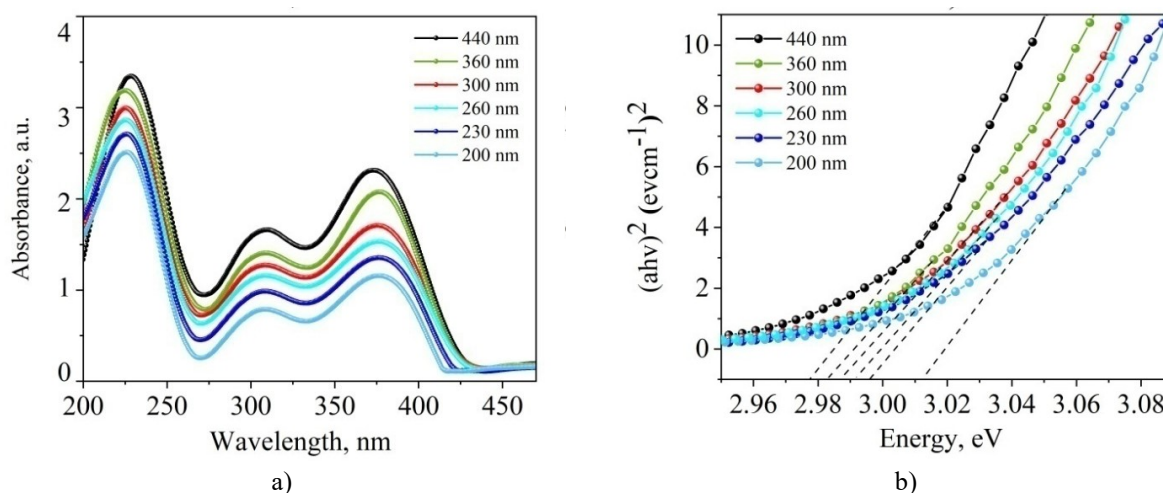
Fig.5. Absorption spectra (a) and band gap (b) Spiro-OMeTAD films with different thicknesses

As the film thickness decreases, a shift in the absorption edge of Spiro-OMeTAD is observed. This shift to short wavelengths is associated with a change in the surface structure of Spiro-OMeTAD films. In addition, decreasing the film thickness leads to a decrease in the optical density of Spiro-OMeTAD.

From the absorption spectra of the films, the energy gap (E_g) of Spiro-OMeTAD was determined using the TaucPlot method (Figure 5 b). Analysis of the data shows that with a decrease in film thickness, an increase in the band gap is observed, respectively, from $E_g = 2.97$ eV to Eg = 3.01 eV. The optical characteristics of Spiro-OMeTAD films are presented in Table 1.

Table 1. Optical characteristics of the Spiro-OMeTAD transport layer at different thicknesses

Film thickness, nm	D_1, A.U. (λ=228 nm)	D_2, A.U. (λ=308 nm)	D_3, A.U. (λ=373 nm)	Bandgap, eV
440	3.49	1.68	2.39	2.977
360	3.39	1.41	2.13	2.982
300	3.03	1.23	1.72	2.987
260	2.95	1.14	1.54	2.991
230	2.79	0.96	1.35	2.995
200	2.57	0.73	1.14	3.012

3.3. Electrophysical characterizations

To study the current-voltage characteristics, perovskite solar cells with the $FTO/TiO_2/CH_3NH_3I_3PbClx/Spiro-OMeTAD/Ag$ structure with different HTL layer thicknesses were constructed. To study the effect of Spiro-OMeTAD thickness on photovoltaic properties, solar cell layers were prepared under the same conditions except for the Spiro-OMeTAD layer. The current-voltage characteristics of PSCs and the energy diagram of the components are presented in Figure 6. From Figure 6 and Table 2 it can be seen that with a decrease in the thickness of the Spiro-OMeTAD film from 200 to 230 nm, an increase in the transmission coefficient of up to 8.6% is observed. The solar cell with Spiro-OMeTAD, obtained with an HTL layer thickness of 260 nm, showed the highest energy conversion efficiency characteristics, reaching 9%. Further increase in the thickness of the Spiro-OMeTAD layer to 440 nm. results in lower photovoltaic performance values of PCSs compared to cells with thin layers of Spiro-OMeTAD.
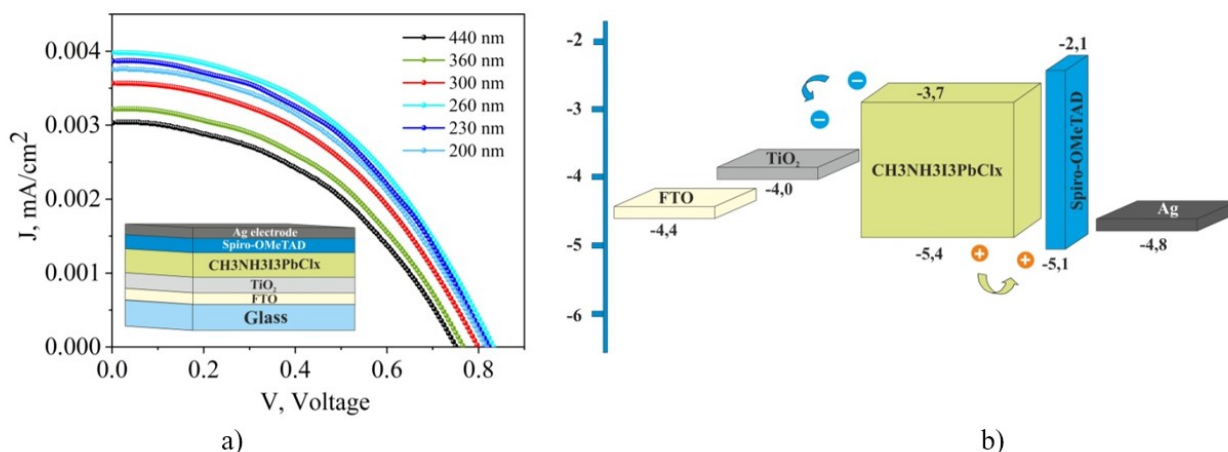

Fig.6. Current-voltage characteristics (a) and energy diagram (b) of perovskite solar cells

The current-voltage characteristics show that the current density increases with increasing Spiro-OMeTAD thickness; the highest current density value $J_{sc} = 24.94$ mA/cm^2 is found in PSCs with a Spiro-OMeTAD film with a thickness of 260 nm. A further decrease in the thickness of the HTL films leads to a decrease in the current density to the value $J_{sc} = 23.41$ mA/cm^2. The findings indicate that the optimal thickness of Spiro-OMeTAD, obtained at a thickness of 260 nm, increases the charge transfer efficiency and reduces the recombination of charge carriers in the transport layer of PSCs.

The change in fill factor (FF) with Spiro-OMeTAD thickness is an indication of a change in series resistance. As the Spiro-OMeTAD thickness decreases to 260 nm, cell efficiency increases from 6.0% to 9.0% due to an increase in fill factor from 0.43 to 0.47 (Table 2). Further reduction in thickness from 230 to 200 nm. Reduces the fill factor to 0.46 and efficiency to 8.3%, respectively.

Table 2. Photovoltaic characteristics of perovskite solar cells

Film thickness, nm	V_{oc}(V)	J_{sc}(mA/cm^2)	V_{max} (V)	J_{max}(mA/cm^2)	FF	PCE %
440	0.74	19	0.50	12.6	0.43	6.0
360	0.76	20.1	0.51	13.5	0.44	6.8
300	0.80	22.3	0.53	14.8	0.45	7,8
260	0.83	24.9	0.55	16.5	0.47	9.0
230	0.82	24.1	0.54	16.1	0.46	8.6
200	0.81	23.4	0.54	15.5	0.46	8.3

To understand the influence of the thickness of the HTL layer of Spiro-OMeTAD on the charge carrier transport mechanisms, measurements of the impedance spectra of PSCs were carried out (Figure 7a). The impedance spectra were analyzed using standard equivalent electrical circuitry, where R_s is the high-frequency resistance, R_{rec} is the low-frequency bulk recombination resistance, and CPE is the phase constant between layers (Figure 7a - insert).
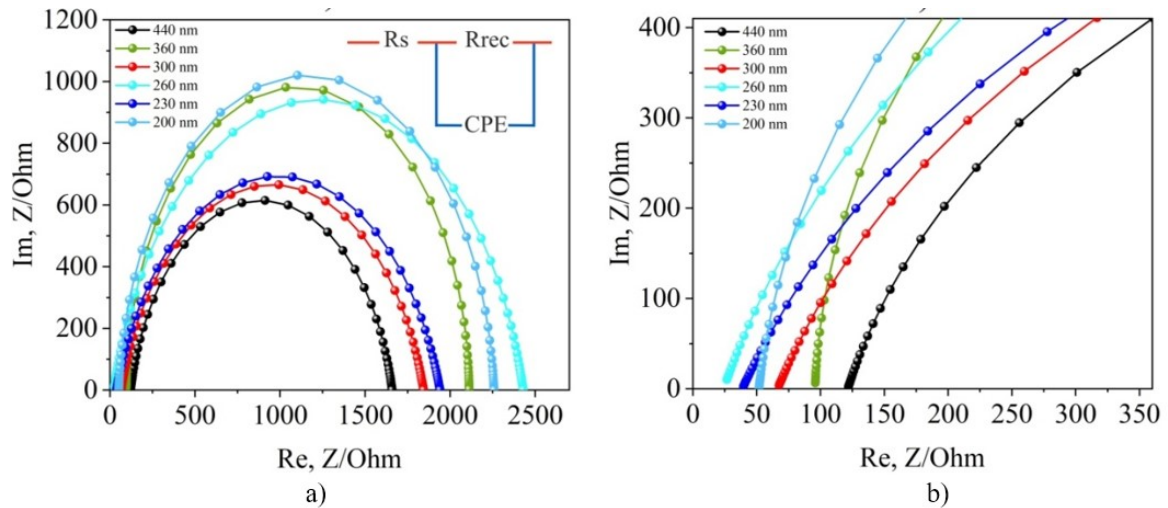

Fig.7. Impedance hodographs in Nyquist coordinates (a) for PSCs with different Spiro-OMeTAD thicknesses, equivalent electrical circuit in the inset; (b) enlarged image of the initial values of the impedance hodographs

The value of the effective charge carrier recombination rate k_{eff} was determined from the maximum arc of the hodograph using the formula:

$$\omega_{eff} = k_{eff} \tag{1}$$

$$\omega = 1/rc,$$

where is angular frequency, rc is a time characteristic of a simple electrical circuit in which the charge of capacitor C changes due to its discharge through resistance R.

The effective lifetime of charge carriers in films is calculated using the formula:

$$\tau_{eff} = 1/k_{eff} \tag{2}$$

The effective free path of charge carriers was calculated using the formula:

$$D_{eff}=R_s/R_{rec} \cdot k_{eff} \cdot L^2 , \hspace{5cm} (3)$$

where L is the film thickness.

As a result of the analysis of impedance spectra, the following electrical transport characteristics were determined: R_s – a parameter characterizing the series resistance of all functional layers of the cell; R_k is the resistance characterizing the recombination channels of charge carriers; τ_{eff} is the effective lifetime of charge carriers, Table 3 shows the parameters listed. P - parameter of constant phase element (CPE), preexponential factor, n is the number of points in the impedance spectrum. Figure 7 b shows an enlarged image of the initial values of the hodographs characterizing the values of the parameter R_s.

Table 3. Parameters of charge injection and transport in perovskite solar cells

Film thickness, nm	R_s, Ohm	R_k, Ohm	R_k/R_s	n	P	k_{eff}, s^{-1}	τ_{eff}, ms
440	121.9	1537.6	12.6	0.86	$1.18*10^{-8}$	501.1	1.9
360	96.1	2016.1	20.9	0.98	$3.25*10^{-9}$	251.1	3.9
300	67.5	1777.8	26.3	0.81	$1.67*10^{-8}$	645.6	1.5
260	26.7	2405.4	90.1	0.84	$2.38*10^{-8}$	158.5	6.3
230	39.6	1901.6	48.1	0.80	$3,33*10^{-8}$	301.9	3.3
200	51.9	2206.1	42.5	0.95	$5.80*10^{-9}$	234.4	4.3

As can be seen from Table 3, the R_s value is the lowest for a cell with a Spiro-OMeTAD HTL layer with a thickness of 260 nm. Further increase in layer thickness leads to an increase in the value of R_s. Since all functional cell layers were obtained under the same conditions, the decrease in R_s is due to the improvement in the efficiency of injection and hole transport. As can be seen from the energy diagram in Figure 6 (b), the positions of the $CH_3NH_3I_3PbCl_x$ cost center are more negative compared to the Spiro-OMeTAD cost center, which generates a stronger built-in electric field for efficient extraction of holes into the anode.

Resistance R_k is also an important parameter characterizing the recombination of charge carriers. From the fitting data it follows that R_k has a low value for cells with a Spiro-OMeTAD HTL layer with a thickness of 440 nm. As the HTL thickness decreases, R_k for cells with an HTL layer of Spiro-OMeTAD at a thickness of 360 nm. and 300 nm increased by 30% and 15%, respectively. At an HTL thickness of 260 nm, R_k reached a maximum value of 2405.4 Ohm, which led to an increase in the resistance efficiency in the charge carrier recombination channels. With further reduction in thickness to 200 nm. there is a decrease in the value of R_k, which in turn leads to a deterioration in the performance of the solar cell. Thus, the Spiro-OMeTAD film, with a thickness of 260 nm, contributes to efficient electron blocking.

A significant increase in the effective lifetime of charge carriers (τ_{eff}) is three orders of magnitude higher for films with a thickness of 260 nm. The significant increase in τ_{eff} can be explained by a decrease in the recombination of charge carriers due to the blocking effect and partly by an improvement in hole transport. When comparing the photovoltaic and electrical transport parameters of cells with an HTL layer of Spiro-OMeTAD, with a thickness of 200 nm up to 440 nm, the following features are observed: a cell with an HTL layer with a thickness of 260 nm. showed an efficiency of 40% more compared to a cell with an HTL layer with a thickness of 440 nm, which is largely due to an increase in photovoltage and fill factor. In cells of the $ITO/TiO_2/CH_3NH_3I_3PbCl_x/Spiro-OMeTAD/Ag$ structure, the photovoltage is caused by the difference between the Fermi level of electrons in TiO_2 and the Fermi level of Spiro-OMeTAD holes. The lower position of the quasi-Fermi level of the Spiro-OMeTAD holes gives an increase in the observed photovoltage. The higher fill factor is largely due to the lower R_s. According to the impedance spectra, the lifetime of charge carriers in a cell with a Spiro-OMeTAD HTL layer with a thickness of 260 nm is almost 3 times greater than τeff in a cell with a Spiro-OMeTAD HTL layer with a thickness of 430 nm. As described earlier, the optical band gap width of a hole-transport layer film with a thickness of 260 nm is almost 0.02 eV greater than that of a film with a thickness of 440 nm, which is due to the lower position of the valence band maximum. This generates a stronger built-in electric field to effectively extract holes into the anode, thereby reducing the likelihood of charge carrier recombination.

Figure 8 shows images of the surface and current distribution of Spiro-OMeTAD on the surface of the peroskite layer. The use of conductive-AFM (CAFM) made it possible to identify a significantly inhomogeneous current distribution on the surface of the samples. In addition to inhomogeneities associated with the perovskite structure, current images of some samples show spots with increased conductivity, which stand out sharply against the general background and are located along the boundaries of crystallites.It was shown in [23] that when this type of AFM is used, the probe-sample contact area is illuminated by the microscope laser. The instrument used to measure the current distributions shown in Figure 8 uses a laser with a wavelength of 650 nm, which falls within the absorption spectrum of the perovskite used in the work.

Thus, the contrast in Figures 8b and 8d contains both dark current and potentially photocurrent. The observed spots of increased conductivity can presumably be interpreted as perovskite quantum dots, which have better photovoltaic characteristics compared to the bulk material. For this reason, research into perovskite quantum dots is currently being actively carried out [24, 25]. We do not know the results of direct observation of the electrical properties of perovskite quantum dots; therefore, our results may be the first visualization of the current distribution on quantum dots.
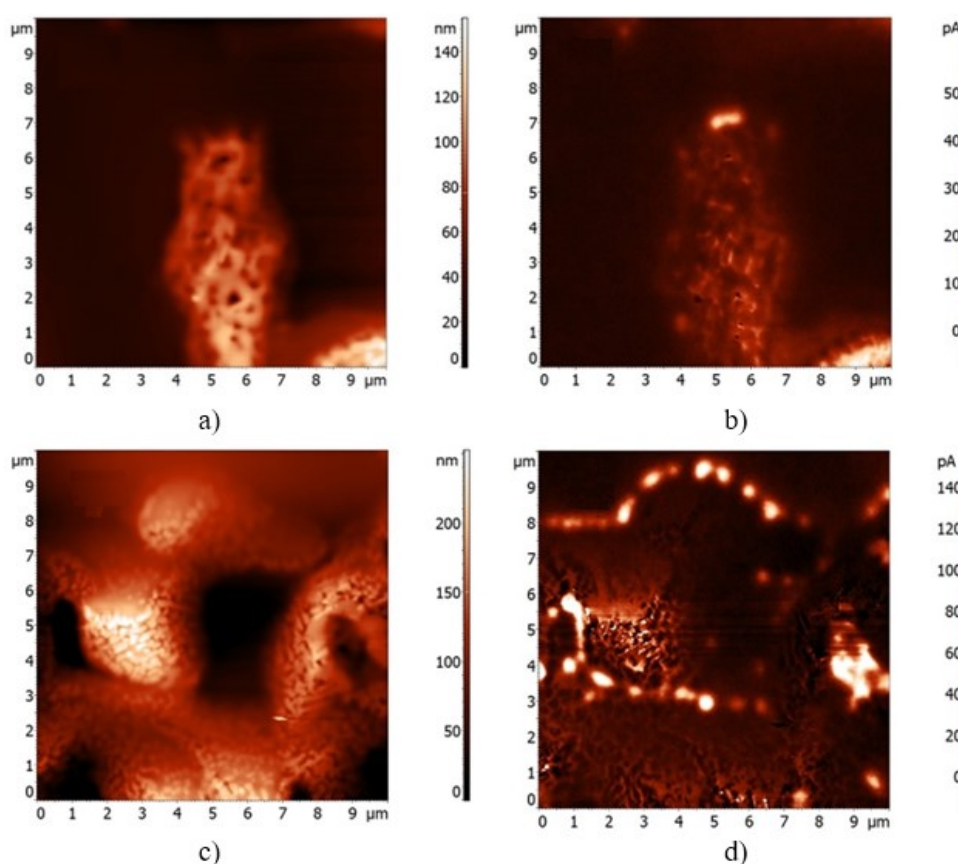

Fig.8. Images of the surface (a, c) and current distribution (b, d). Samples obtained at different centrifuge rotation speeds: a, b) – 2000 rpm, c, d) –5000 rpm. Images of the surface (a, c) and current distribution at a voltage across the sample of +5 V (b, d)

From the data obtained, we can make an assumption about the possible influence of the number of quantum dots on the efficiency of the resulting cells: the largest number of them was observed in sample 4, which shows an efficiency close to the maximum (see Table 2). At the same time, the small size of the scanning area of the AFM used in the work does not allow us to estimate the statistics of the distribution of quantum dots over the samples. Currently, the authors are conducting a more detailed study of perovskite quantum dots using electrical AFM methods.

4. Conclusions

In these studies, perovskite solar cells with FTO/TiO$_2$/CH$_3$NH$_3$I$_3$PbCl$_x$/Spiro-OMeTAD/Ag architecture were fabricated. The effect of the Spiro-OMeTAD layer density on the photovoltaic characteristics of PSCs was investigated.

The Spiro–OMeTAD hole-transport layer was obtained by the Spin-coating method. The thickness of the Spiro–OMeTAD layer was controlled by changing the centrifugation rotation speed. It was revealed that a monotonic decrease in the thickness of the Spiro–OMeTAD film leads to a sharp increase in the rms of the surface when the rotation speed increases to 4000 rpm, then the dependence saturates.

The dependences of thickness and rms on rotation speed for films on FTO are inversed: $\sim 1/w^{0.5}$ and $\sim w^{0.5}$, correspondingly. As the film thickness decreases, a decrease in the optical absorption density in the spectrum and an increase in the optical band gap of Spiro–OMeTAD films are observed. Electrical impedance spectra were measured for PSCs with different Spiro-OMeTAD thicknesses. It is shown that the series resistance of the functional layers of the cell depends on the thickness of the Spiro–OMeTAD layer. With thin layers, a decrease in resistance is observed; the lowest value is observed in a cell with an HTL layer of Spiro-OMeTAD with a thickness of 260 nm. A further increase in the thickness of the layer leads to an increase in resistance.

The use of conductive-AFM (CAFM) made it possible to identify a significantly inhomogeneous current distribution on the surface of the samples. In addition to inhomogeneities associated with the perovskite structure, current images of some samples show spots with increased conductivity, which stand out sharply against the general background and are located along the boundaries of crystallites. The observed spots of increased conductivity can presumably be interpreted as perovskite quantum dots, which have better photovoltaic characteristics compared to the bulk material.

References

1 Devadiga D., Nagaraja A.T., Devadiga Dh., Selvakumar M. (2024) Minireview and Perspectives of Liquid Crystals in Perovskite Solar Cells. *Energy & Fuels*, 38 (2), 854 - 868. DOI: 10.1021/acs.energyfuels.3c04050.

2 Sha W.E.I., Ren X., Chen L., Choy W.C.H. (2015) The efficiency limit of CH$_3$NH$_3$PbI$_3$ perovskite solar cells. *Appl. Phys. Lett.*, 106, 221104. DOI: 10.1063/1.4922150.

3 Saliba M., Correa-Baena J.-P., Gratzel M., Hagfeldt A., Abate A. (2018) Perovskite Solar Cells: From the Atomic Level to Film Quality and Device Performance. *Angew. Chem., Int. Ed.*, 57, 2554–2569. DOI:10.1002/anie.201703226.

4 Aristidou N., Eames C., Sanchez-Molina I., Bu X., Kosco J., Islam M. S., Haque S.A. (2017) Fast oxygen diffusion and iodide defects mediate oxygen-induced degradation of perovskite solar cells. *Nat. Commun.*, 8, 15218. DOI: 10.1038/ncomms15218.

5 Wolff C.M., Caprioglio P., Stolterfoht M., Neher D. (2019) Nonradiative Recombination in Perovskite Solar Cells: The Role of Interfaces. *Adv. Mater.*, 31, 1902762. DOI: 10.1002/adma.201902762.

6 Jeong J., Kim M., Seo J., Lu H., Ahlawat P., Mishra A., Yang Y., Hope M. A., Eickemeyer F.T., Kim M., Yoon Y. J., Choi I. W., Darwich B.P., Choi S. J., Jo Y., Lee J. H., Walker B., Zakeeruddin S.M., Emsley L., Rothlisberger U., Hagfeldt A., Kim D. S., Gra¨tzel M., Kim J.Y. (2021) Pseudo-halide anion engineering for a-FAPbI3 perovskite solar cells. *Nature*, 592, 381–385.DOI: 10.1038/s41586-021-03406-5.

7   Guan-Woo K., Hyuntae C., Minjun K., Lee J., Son S.Y., Park T. (2020) Hole transport materials in conventional structural (n-i-p) perovskite solar cells: from past to the future. *Adv Energy Mater.*, DOI:10.1002/aenm.201903403.

8   Jeyakumar R., Bag A., Nekovei R., Radhakrishnan R. (2019) Interface studies by simulation on methylammonium lead iodide based planar perovskite solar cells for high efficiency. *Sol. Energy*, 104-111. DOI:10.1016/j.solener.2019.07.097.

9   Tumen-Ulzii G., Matsushima T., Adachi C. (2021) Mini-Review on Efficiency and Stability of Perovskite Solar Cells with Spiro-OMeTAD Hole Transport Layer: Recent Progress and Perspectives. *Energy & Fuels,* 35 (23), 18915-18927. DOI: 10.1021/acs.energyfuels.1c02190.

10   Yoo J.J., Wieghold S., Sponseller M.C., Chua M. R., Bertram S.N., Hartono N.T.P., Tresback J.S., Hansen E.C., Correa-Baena J.-P., Bulovic´V., Buonassisi T., Shin S.S., Bawendi M.G. (2019) An interface stabilized perovskite solar cell with high stabilized efficiency and low voltage loss. *Energy Environ. Sci.*, 12, 2192–2199. DOI:10.1039/C9EE00751B.

11   Jiang Q., Zhao Y., Zhang X., Yang X., Chen Y., Chu Z., Ye Q., Li X., Yin Z., You J. (2019) Surface passivation of perovskite film for efficient solar cells. *Nat. Photonics,* 13, 460–466. DOI: 10.1038/s41566-019-0398-2.

12   Stolterfoht M., Caprioglio P., Wolff C., Ma´rquez Prieto J., Nordmann J., Zhang S., Rothhardt D., Ho¨rmann U., Amir Y., Redinger A., Kegelmann L., Zu F., Albrecht S., Koch N., Kirchartz T., Saliba M., Unold T., Neher D. (2019) The impact of energy alignment and interfacial recombination on the internal and external open-circuit voltage of perovskite solar cells. *Energy Environ. Sci.,* 12, 2778–2788. DOI: 10.1039/C9EE02020A.

13   Hawash Z., Ono L. K., Qi Y. (2018) Recent Advances in SpiroMeOTAD Hole Transport Material and Its Applications in Organic-Inorganic Halide Perovskite Solar Cells. *Adv. Mater. Interfaces*, 5, 1700623. DOI: 10.1002/admi.201700623.

14   Gelmetti, Montcada N., Pe´rez-Rodrı´guez A., Barrena E., Ocal C., Garcı´a-Benito I., Molina-Ontoria A., Martı´n N., Vidal-Ferran A., Palomares E. (2019) Energy Alignment and Recombination in Perovskite Solar Cells: Weighted Influence on the Open Circuit Voltage. *Energy Environ. Sci.,* 12, 1309–1316. DOI: 10.1039/C9EE00528E.

15   Wolff C.M., Caprioglio P., Stolterfoht M., Neher D. (2019) Nonradiative Recombination in Perovskite Solar Cells: The Role of Interfaces. *Adv. Mater.*, 31, 1902762. DOI: 10.1002/adma.201902762.

16   Wang J., Liu K., Ma L., Zhan X. (2016) Triarylamine: Versatile Platform for Organic, Dye-Sensitized, Perovskite Solar Cells. *Chem. Rev.*, 116, 14675–14725. DOI: 10.1021/acs.chemrev.6b00432.

17   Le Corre V.M., Stolterfoht M., Perdigo´n Toro L., Feuerstein M., Wolff C., Gil-Escrig L., Bolink H. J., Neher D., Koster L. J. A. (2019) Charge Transport Layers Limiting the Efficiency of Perovskite Solar Cells: How To Optimize Conductivity, Doping, and Thickness. *ACS Appl. Energy Mater.*, 2, 6280–6287. DOI:10.1021/acsaem.9b00856.

18   Grill I., Aygu¨ler M. F., Bein T., Docampo P., Hartmann N. F., Handloser M., Hartschuh A. (2017) Charge Transport Limitations in Perovskite Solar Cells: The Effect of Charge Extraction Layers. *ACS Appl. Mater. Interfaces,* 9, 37655–37661. DOI: 10.1021/acsami.7b09567.

19   Stolterfoht M., Wolff C. M., Amir Y., Paulke A., Perdigon L., Caprioglio P., Neher D. (2017) Approaching the Fill Factor Shockley Queisser Limit in Stable, Dopant-Free Triple Cation Perovskite Solar Cells. *Energy Environ. Sci.,* 10, 1530. DOI: 10.1039/C7EE00899F.

20   Das A.K., Mandal R., Mandal D.K. (2022) Impact of HTM on Lead-free Perovskite Solar Cell with High Efficiency. *Optical and Quantum Electronics,* 07. DOI: 10.1007/s11082-022-03852-z.

21   Bag A., Radhakrishnan R., Nekovei R., Jeyakumar R. (2020) Effect of absorber layer, hole transport layer thicknesses, and its doping density on the performance of perovskite solar cells by device simulation. *Solar Energy,* 196, 177-182. DOI: 10.1016/j.solener.2019.12.014.

22   Da Y., Xuan Y., Li Q. (2018) Quantifying energy losses in planar perovskite solar cells. *Sol. Energy Mater. Sol. Cells,* 174, 206–213. DOI: 10.1016/j.solmat.2017.09.002.

23   Aimukhanov A.K., Rozhkova X.S., Ilyassov B.R., Omarbekova G.I., Seisembekova T.E. (2022) Effect of alcohol solvents on the structural, optical and electrical characteristics of PEDOT:PSS polymer films annealed at low atmospheric pressure. *Eurasian physical technical journal,* 19, 2 (40), 35-41. DOI: 10.31489/2022No2/35-41.

24   Hedley G., Ward A., Alekseev A., Calvyn T., Howells E.R., Serrano L., Cooke G., Ruseckas A., Samuel I.D. (2013) Determining the optimum morphology in high-performance polymer-fullerene organic photovoltaic cells. *Nature Communications,* 4, 2867. DOI:_10.1038/ncomms3867.

25   Han R., Zhao Q., Hazarika A., Li J., Cai H., Ni J., Zhang J. (2022) Ionic Liquids Modulating CsPbI3 Colloidal Quantum Dots Enable Improved Mobility for High-Performance Solar Cells. *ACS Appl. Nano Mater.*, 5, 10, 14092–14132. DOI: 10.1021/acsami.1c20274.

AUTHORS' INFORMATION

Tazhibayev, Serzhan Kozhanuly – Master (Sci.), Senior lecturer, E.A. Buketov Karaganda University, Karaganda, Kazakhstan. Scopus Author ID: 58170071100; ORCID iD: 0000-0001-9059-2975: tazh1981@gmail.com

Alekseev, Alexander Mikhailovich – Candidate of Phys. and Math. Sciences, Lead engineer, Kazan Federal University, Kazan, Russia. Scopus Author ID: 55286055800, ORCID iD: 0000-0002-2800-6047; alalrus@gmail.com

Aimukhanov, Aitbek Kalievich – Candidate of Phys. and Math. Sciences, Professor, E.A. Buketov Karaganda University, Karaganda, Kazakhstan. Scopus Author ID: 58493008700, ORCID iD: 0000-0002-4384-5164, a_k_aitbek@mail.ru

Ilyassov, Baurzhan Rashidovich – PhD, Associate Professor, Astana IT University, Expo C1, Astana, Kazakhstan. Scopus Author ID: 56669724700; ORCID iD: 0000-0003-4563-2004; baurdinho@mail.ru

Beisembekov, Meirkhan Kurmangazyuly – Master, E.A. Buketov Karaganda University, Karaganda, Kazakhstan. Scopus Author ID: 58984780800; ORCID iD: 0000-0003-2788-1699; baiboldy_han@mail.ru

Rozhkova, Xenia Sergeevna – PhD, Senior Lecturer, E.A. Buketov Karaganda University, Karaganda, Kazakhstan. Scopus Author ID: 57219053347; ORCID iD: 0000-0003-3048-6171; ksusharogovaya@mail.ru

Mussabekova, Assel Kanatkyzy – Master (Eng.), Senior Lecturer, E.A. Buketov Karaganda University, Karaganda, Kazakhstan. Scopus Author ID: 58429663700, ORCID iD: 0000-0003-3452-4622; assel501vremennyi@mail.ru

Zeinidenov, Assylbek Kalkenovich – PhD, Professor, E.A. Buketov Karaganda University, Karaganda, Kazakhstan. Scopus Author ID: 56386144000; ORCID iD: 0000-0001-9232-8406; asyl-zeinidenov@mail.ru